

# Quantified angular contributions for high harmonic emission of molecules in three dimensions

Limor S. Spector<sup>1,2\*</sup>, Maxim Artamonov<sup>3</sup>, Shungo Miyabe<sup>2,4</sup>, Todd Martinez<sup>2,4</sup>, Tamar Seideman<sup>3</sup>, Markus Guehr<sup>2</sup>, and Philip H. Bucksbaum<sup>1,2</sup>

<sup>1</sup>*Applied Physics Department, Stanford University, Stanford, CA 94305, USA*

<sup>2</sup>*Stanford PULSE Institute, SLAC National Accelerator Laboratory, Menlo Park, CA 94025, USA*

<sup>3</sup>*Department of Chemistry, Northwestern University, Evanston, Illinois 60208, USA*

<sup>4</sup>*Chemistry Department, Stanford University, Stanford, CA 94305, USA*

(Received 10 July 2012)

We study high-order harmonic generation (HHG) in impulsively aligned quantum asymmetric tops. We quantify the angular contributions of HHG emission, making use of the full rotational revival structure. We find a signal sensitive to all five prolate top revival types and to fractional and multiple revivals, providing a new view of polyatomic rotations. Our results show that not only the HOMO orbital shape, but also the orientation dependence of the recombination dipole controls the harmonic efficiency. This has implications for HHG-based tomographic imaging.

PACS numbers: 42.50.Hz, 33.80.-b, 42.65.Re, 33.20.Sn

The ability to directly image the structure of the outermost electrons in molecules, and thereby view chemical reactions as they occur, is an important goal in molecular physics and chemistry today. For molecules with three distinct axes of rotation, known as asymmetric top molecules, this goal of electron tomography can only be realized by disentangling the signal coming from each of the three molecular axes. Since most molecules are asymmetric tops, the challenge of resolving the contributions of the different molecular rotations to the experimental signal is one that confronts much of the ultrafast science community, including users of techniques like time-resolved time-resolved x-ray [1, 2] and electron diffraction [3, 4], photoelectron spectroscopy [5, 6], and high harmonic generation (HHG) [7-9]. HHG, in particular, has shown promise as a technique for tomographic reconstruction [10], and there have been significant advances in understanding the high harmonic signal arising from a linear molecule [11, 12]. Here we describe a new method based on quantum revivals to observe the strong-field laser-molecule interaction in the body frame of an asymmetric top molecule. Specifically, we quantify the high harmonic dependence on molecular orientation for laser polarizations aligned with each of the three principal axes in the molecule.

As a test case for our method we chose sulfur dioxide (SO<sub>2</sub>), which is a small asymmetric top molecule. We examine the full rotational revival structure of SO<sub>2</sub> and observe all types of rotational revivals, as well as fractional and multiple revivals, which have not previously been seen [13]. Such high sensitivity to impulsive revivals appears to be a feature of HHG. HHG has recently been shown to be a particularly sensitive technique for measuring alignment [14, 15], and recent calculations

predict that all axes undergo periodic angular focusing effects [16]. We simulate the alignment with respect to each of the molecular axes and combine the simulations to determine the amount of high harmonic emission arising from each direction in our data. The revival structures serve as snapshots in time when the molecule is aligned in space in different directions, which we can use to pick out and quantify the particular angular contributions without employing complicated experimental schemes, like three-dimensional alignment [17]. Through the revival structure we are also able to learn about how the electron orbital shape of SO<sub>2</sub> affects the efficiency of the high harmonics. Our method is generalizable to any molecule that can exhibit revivals, including a wide class of asymmetric tops. The goal of HHG-based electron tomography has received much attention [10, 18-21], and this result brings us closer to this goal for more complex molecules, while at the same time suggesting a new approach to understanding the rotations of complex polyatomic molecules and hence their structural properties.

The experimental scheme employs impulsive stimulated rotational Raman scattering for alignment. We use one 130 fs pulse at 800 nm with an intensity in the 10<sup>13</sup> W/cm<sup>2</sup> range to impulsively align a sample of SO<sub>2</sub> molecules. We probe the SO<sub>2</sub> at various time delays by using a focused 30 fs pulse at 800 nm with an intensity of approximately 2.6 x 10<sup>14</sup> W/cm<sup>2</sup> to produce HHG in the SO<sub>2</sub> gas. Both laser beams are linearly polarized parallel to each other. The molecules are introduced through a nozzle located above the laser focus and thus slightly cooled to approximately 240K at the laser focus. Following the alignment pulse, the SO<sub>2</sub> is free to rotate, exhibiting a revival structure that is determined by the field-free rotational spectrum. We vary the time delay between the

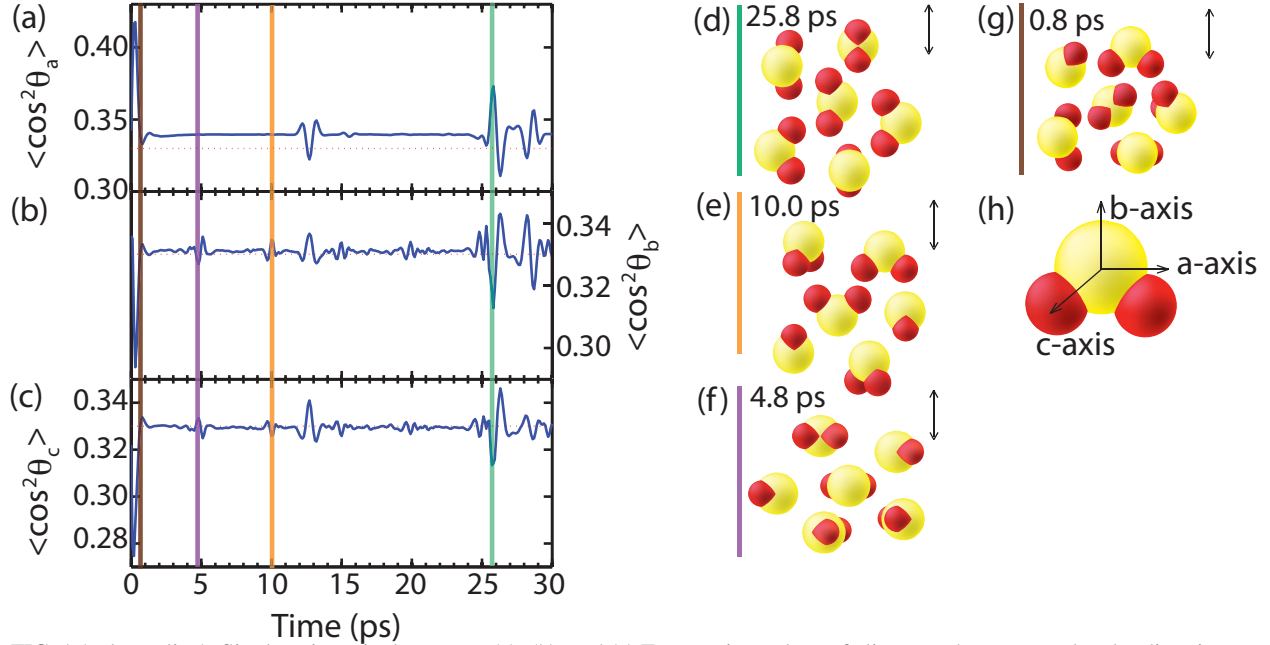


FIG. 1 (color online). Single axis revival patterns. (a), (b), and (c) Expectation values of alignment between molecular directions a, b, and c and the polarization direction of the HHG probing pulse. The molecules are in an isotropic distribution for  $\langle \cos^2 \theta \rangle = 0.33$ . (d), (e), (f), and (g) Idealized sample distributions at different revival times. The laser polarization direction is indicated. (d)-(f) correspond to alignments along axes a, b and c, respectively. (h) Molecular axes for  $\text{SO}_2$ .

two pulses between 0 and 30 ps. This allows us to record the transient alignment revivals. The HHG is dispersed through a flat-field diffraction grating spectrometer and amplified with a microchannel plate and detected on a phosphor screen. Since the  $\text{SO}_2$  molecules are aligned with respect to the field polarization vector at a molecular revival, the harmonic signal is sensitive to the molecular structure along the revival axis.

Figures 1(a)-1(c) shows calculations of molecular alignment with respect to all three molecular axes, where a, b, and c refer to those molecular axes shown in Fig. 1(h). We show the expectation value of  $\cos^2 \theta_i$  in the rotational wavepacket, where  $\theta_i$  is the angle between the polarization direction of the HHG probing pulse and the molecular axis  $i$ . The a-axis (along the O-O vector) is the most polarizable axis of the molecule and the b-axis ( $C_{2v}$ ) is the molecular symmetry axis. An isotropic ensemble has an expectation value of 0.33, as depicted by a dashed red line in the figure.

The aligning pulse duration and intensity in the calculation are taken to be the same as used in our experiments, and the observables are calculated for a thermal ensemble corresponding to the temperature of 180K, the highest temperature that was computationally feasible. Our theory and numerical approach for solving the time-dependent Schrödinger equation of an asymmetric top molecule interacting with an aligning field are described in detail in [22] and [23]. In brief, for the duration of the laser pulse, the rotational wavefunction is expanded in a symmetric top basis,  $|JKM\rangle$ , thus converting the

time-dependent Schrödinger equation into a set of coupled differential equations that are solved numerically. Here J, K, and M denote the quantum numbers corresponding to the total angular momentum and its projections onto the body- and space-fixed axes. Because the aligning pulse is linearly polarized, the wavefunction is effectively two-dimensional with only parametric dependence on M. Note that K is not a conserved quantum number for an asymmetric top. The pulse is modeled as a Gaussian. After the pulse turn-off, when the envelope tail is truncated as it becomes sufficiently small, the wavefunction is transformed to the basis of eigenstates of the field-free Hamiltonian.

Figure 1 demonstrates that at different times different axes are aligned with respect to the laser polarization. The three alignment curves taken together show the time variation of molecular alignment. If the rotational distribution with respect to one axis is peaked, whereas the other two are not, the molecule is partially aligned along that axis at that time. Figures 1(d)-1(f) show example alignments along the molecular axes a, b, and c with respect to the laser polarization. Figure 1(g) shows an isotropic molecular distribution. The principal components of the polarizability tensor were determined in [24].

Our data of the 19<sup>th</sup> harmonic is shown in Fig. 2(b). As expected based on the discussion above, the revival structure is complex, that is, the molecules shows revivals about all axes. While linear and symmetric top molecules exhibit complete periodic revivals, asymmetric top molecules undergo classically unstable motion and hence

do not exhibit complete reconstruction of the initial state. A few structures are immediately apparent in Fig. 2(b): there is an initial alignment peak immediately following the impulse with a duration of less than 1 ps. A revival peak appears around 12 ps as well as a large and complex triply-peaked revival structure around 26 ps. In addition, we see smaller peaks around multiples of 4 ps, and very closely spaced peaks representing vibrational coherences, particularly in the early part of the spectrum.

The different types of rotations in  $\text{SO}_2$  that are responsible for these revivals are conveniently characterized using the nomenclature developed in rotational coherence spectroscopy [25], although our present strong field, far-off-resonance excitation gives rise to qualitatively different rotational wavepackets. Asymmetric tops are classified as near-oblate or near-prolate in analogy with symmetric top molecules. As a near-prolate asymmetric top molecule,  $\text{SO}_2$  is expected to exhibit J-type and K-type revivals corresponding to quasi-symmetric-top-like rotations. Since  $\text{SO}_2$  is, however, an asymmetric top, it can also exhibit A-type, C-type and Hybrid-type revivals.

The extensive results of rotational coherence spectroscopy allow us to compute the revival times for  $\text{SO}_2$  [26]. A summary of these appears in Table I. We can identify partial and full J-type revivals at 13 and 26 ps, respectively, a C-type revival at 28 ps, and several A-type,

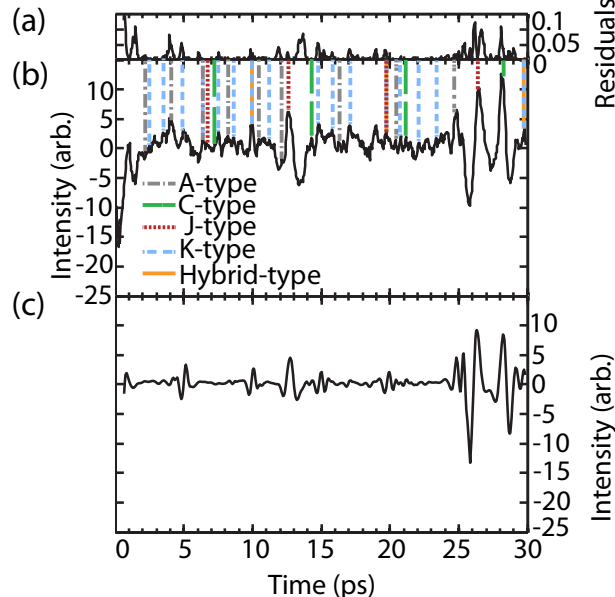


FIG. 2 (color online). Comparison between experiment and a best-fit theory curve. (a) Residuals between experiment and best-fit theory. (b) Data for high harmonic 19 (29.5 eV) for the first 30 ps following alignment. Harmonic intensity is arbitrary. Several revivals are shown with vertical lines, and identification of these revivals is done in Table I. The high harmonic data is very sensitive to  $\text{SO}_2$  revivals, with order up to 1/16 revivals visible. (c) Best-fit theory curve fits all 3 single-axis revival patterns to the data, yielding quantitative information about the angles from which HHG emission originated.

K-type, and Hybrid-type revivals at multiples of 4, 5 and 10 ps, respectively, except for where they are masked by the partial revival signature. We also see other partial revivals, of order up to 1/16 revivals. All revivals are shown on Fig. 2(b) using vertical lines. To our knowledge, this is the first time impulsive revivals of all rotations of an asymmetric top molecule have been seen in a single revival pattern.

This experiment shows a very high level of sensitivity to rotational revivals. In the pioneering work of Lee et al.,  $\text{SO}_2$  was aligned along two of its three axes, but alignment was inferred using only the initial alignments with no revivals reported [13]. Rotational revivals have only been seen in a few asymmetric top molecules and usually only at very low temperatures [27].

Each rotation in the asymmetric top has a unique revival signature. In particular, the three *single-axis* revival patterns are shown in Fig. 1(a)-(c). We can extract the harmonic signal along each of the principal axes of the molecule by combining these to form a best fit to the data. We used a 4-parameter Nelder-Mead procedure to optimize the fit. The result is shown in Fig. 2(c) and the residuals are shown in Fig. 2(a).

	A-type	C-type	J-type	K-type	Hybrid
1/4	1.0	<b>7.1</b>	<b>6.5</b>	1.2	2.4
1/2	<b>2.1</b>	<b>14.2</b>	<b>13.1</b>	<b>2.4</b>	4.9
3/4	3.1	<b>21.3</b>	<b>19.6</b>	<b>3.7</b>	7.3
Full	<b>4.1</b>	<b>28.4</b>	<b>26.2</b>	<b>4.9</b>	<b>9.8</b>
1 1/4	5.1	35.5	32.7	<b>6.1</b>	12.2
1 1/2	<b>6.2</b>	42.6	39.2	<b>7.3</b>	14.6
1 3/4	7.2	49.7	45.8	<b>8.5</b>	17.1
2nd	<b>8.2</b>	56.8	52.3	<b>9.8</b>	<b>19.5</b>
2 1/4	9.3	63.9	58.8	<b>11.0</b>	22.0
2 1/2	<b>10.3</b>	71.0	65.4	12.2	24.4
2 3/4	11.3	78.1	71.9	13.4	26.8
3rd	<b>12.3</b>	85.2	78.5	<b>14.6</b>	<b>29.3</b>
3 1/4	13.4	92.3	85.0	<b>15.9</b>	31.7
3 1/2	14.4	99.4	91.5	<b>17.1</b>	34.2
3 3/4	15.4	106.5	98.1	18.3	36.6
4th	<b>16.5</b>	113.6	104.6	<b>19.5</b>	39.0
4 1/4	17.5	120.7	111.1	<b>20.7</b>	41.5
4 1/2	18.5	127.8	117.7	<b>22.0</b>	43.9
4 3/4	19.5	134.9	124.2	<b>23.2</b>	46.4
5th	<b>20.6</b>	142.0	130.8	24.4	48.8
6th	<b>24.7</b>	170.5	156.9	<b>29.3</b>	58.6

Table I: Expected revivals for  $\text{SO}_2$  (in ps). Numbers in bold indicates that they are marked with a vertical line in Fig. 2(b).

We expect harmonic generation to have a nonlinear dependence on geometry, since the field-ionization step in the standard semi-classical model of the process is very sensitive to small changes in the charge density at the laser-induced saddle point in the potential, and is also sensitive to the recombination dipole moment. This analysis does not attempt to model this in detail, but we do find that the data show rotational revivals that are much more prominent than the model. For example, the A-type revival seen very clearly in the data is barely visible in any of the single-axis revival curves, and is therefore not present in the full analysis. This procedure therefore reveals orientation features in the high harmonic process such as extreme sensitivity to A-type alignment. Alignment distributions calculated specifically for a HHG probe would further refine this method.

The coefficients from the fit show the relative amount of high harmonic emission originating from each molecular direction to obtain the single-molecule angular contributions of SO<sub>2</sub> to HHG. This provides a path towards HHG-based tomographic reconstruction of asymmetric top molecules. The fit coefficients are in a ratio of approximately  $-1 \pm 0.7:128 \pm 1.9:4 \pm 0.8$  for axes a:b:c. Therefore we conclude that emission comes primarily from molecules aligned with the polarization along the C<sub>2v</sub> (b) axis. Our data further indicate that the harmonic emission is suppressed by more than two orders of magnitude at the orientations along the a-axis, where the polarizability is largest.

The high contribution to harmonic emission from the C<sub>2v</sub> (b) axis could be due to either enhanced field ionization or enhanced recombination to the axis, according to the standard recollision model [28-30]. We model the energy- and angle-dependent recombination dipole by calculating the VUV photoemission cross section of SO<sub>2</sub> in the molecular frame. This gives us information about the recombination electron, because the recombination step in HHG is equivalent to inverse photoionization. We computed fixed-nuclei photoionization amplitudes using the complex Kohn variational method [31]. The final-state electronic wavefunction for production of photoions is in a specific cation state. Only one ionic target state, the 8a<sub>1</sub><sup>-1</sup> hole state, was included in the trial wave function. Further details can be found elsewhere [31-33]. Photoionization cross sections in the molecular frame were then constructed from the matrix elements

$$I_{\Gamma_0 l_0 m_0}^{\mu} = \langle \Psi_0 | r^{\mu} | \Psi_{\Gamma_0 l_0 m_0} \rangle,$$

where  $r^{\mu}$  is a component of the dipole operator, which we evaluate here in the length form.  $\Psi_0$  is the initial-state wave function of the neutral  $N$  electron molecule.

Figure 3(a) shows that recombination dynamics are major contributors to the direction of harmonic emission in the molecular frame. In this figure, the three curves correspond to the recombination in three differ-

ent polarization directions. The dotted blue line (a-axis) shows the cross section when the laser is oriented along the most polarizable axis of the molecule, while the solid green line (b-axis) shows the cross section when the laser is oriented along the symmetry axis of the molecule. The dashed red c-axis line shows the cross section along the third molecular axis.

The energy at the 19<sup>th</sup> harmonic is 29.5 eV; looking at that point in Fig. 3(a), we see that while there is a large recombination probability along the molecular symmetry axis, the calculation shows much less recombination probability along the most polarizable axis of the molecule. We compared this to recombination probabilities arising from the other valence orbitals (HOMO-1 through HOMO-5). The recombination dipole dependence on geometry for these orbitals shows that our signal arises primarily from the HOMO. Figure 3(b) shows the HOMO for SO<sub>2</sub>. Since there is greater electron density along the symmetry axis there is a higher recombination probability in the symmetry axis direction. The analysis suggests that the orientation of harmonic emission is largely controlled by the recombination dynamics and hence responds directly to the form of the electronic orbital that dominates recombination.

We have extracted quantitative three-dimensional information about the geometric dependence of HHG in an asymmetric top by exploiting the rich information available in the quantum rotational revivals. We find that HHG is extremely sensitive to molecular alignment and therefore is a powerful probe of molecular geometry. Using HHG, we were able to detect multiple full revivals in SO<sub>2</sub>. We have observed rotations about different axes and can identify all possible revival types in our high harmonic spectra and were able to see partial and multiple revivals in the data, as predicted by theory. We see

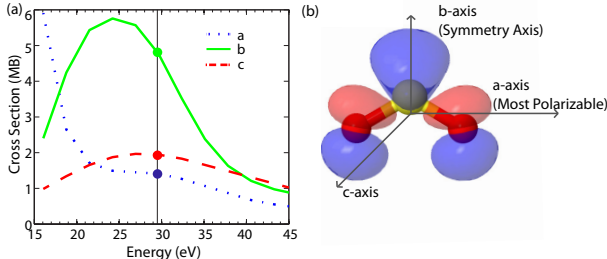


FIG. 3 (color online). (a) Recombination cross section of SO<sub>2</sub> as a function of photon energy. The laser polarization is oriented along the a, b and c axes of the molecule in the dotted blue, solid green, and dashed red curves, respectively. High harmonic 19 has approximately 29.5 eV of energy; at this point the recombination cross section is much higher along the molecular symmetry axis (b-axis) than along either of the other two axes. (b) A sketch of the HOMO of SO<sub>2</sub>, shown in red and blue to encode the phase, overlaid with a ball and stick model. We see highest HHG signal originating from the symmetry axis direction, in confirmation of our analysis.

a strong dependence of the recombination dipole on the HHG signal for  $\text{SO}_2$ . We present a method that uses only a single impulse to extract information about all three axes. This removes the necessity to align a polyatomic molecule along all three dimensions and points the way towards HHG-based tomography in asymmetric tops.

We would like to acknowledge fruitful discussions with Song Wang, Joseph P. Farrell, Brian K. McFarland, Varun Makhija, and Xiaoming Ren. This research is supported through the Chemical Sciences Division of the SLAC National Accelerator Laboratory by the U.S. Department of Energy, Office of Basic Energy Sciences and by a U.S. Department of Energy award (Grant No. DE-FG02-04ER15612). We acknowledge support from a National Defense Science and Engineering Graduate Fellowship (LSS) and a Stanford Diversifying Academia, Recruiting Excellence Graduate Fellowship (LSS).

\*Corresponding Author. LSpector@stanford.edu

- [1] H. N. Chapman *et al.*, *Nature* **470** (2011).
- [2] G. Sciaini *et al.*, *Nature* **458** (2009).
- [3] A. H. Zewail, *Science* **328** (2010).
- [4] C. I. Blaga *et al.*, *Nature* **483** (2012).
- [5] C. Z. Bisgaard *et al.*, *Science* **323** (2009).
- [6] J. L. Hansen *et al.*, *Phys. Rev. Lett.* **106** (2011).
- [7] D. Shafir *et al.*, *Nature* **485** (2012).
- [8] N. Kajumba *et al.*, *New Journal of Physics* **10** (2008).
- [9] W. Li *et al.*, *Science* **322** (2008).
- [10] J. Itatani *et al.*, *Nature* **432** (2004).
- [11] B. K. McFarland *et al.*, *Science* **322** (2008).
- [12] X. Zhou *et al.*, *Phys. Rev. Lett.* **100** (2008).
- [13] K. F. Lee *et al.*, *Phys. Rev. Lett.* **97** (2006).
- [14] R. M. Lock, Ramakrishna, S., Zhou, X., Kapteyn, H.C., Murnane, M.M. and T. Seideman, *Phys. Rev. Lett.* (2012).
- [15] S. Ramakrishna, and T. Seideman, *Phys. Rev. Lett.* **99** (2007).
- [16] S. Pabst, and R. Santra, *Physical Review A* **82** (2010).
- [17] V. Makhija, X. M. Ren, and V. Kumarappan, *Physical Review A* **85** (2012).
- [18] D. Shafir *et al.*, *Nature Physics* **5** (2009).
- [19] E. Hijano *et al.*, *Physical Review A* **81** (2010).
- [20] C. Vozzi *et al.*, *Nature Physics* **7** (2011).
- [21] Y. Chen *et al.*, *Physical Review A* **77** (2008).
- [22] M. Artamonov, and T. Seideman, *Journal of Chemical Physics* **128** (2008).
- [23] T. Seideman, and E. Hamilton, *Advances in Atomic Molecular and Optical Physics*, Vol 52 **52** (2005).
- [24] P. B. Lukins, and G. L. D. Ritchie, *Journal of Physical Chemistry* **89** (1985).
- [25] M. D. Poulsen *et al.*, *Journal of Chemical Physics* **121** (2004).
- [26] P. M. Felker, *Journal of Physical Chemistry* **96** (1992).
- [27] A. Rouzee *et al.*, *Physical Review A* **73** (2006).
- [28] P. B. Corkum, *Phys. Rev. Lett.* **71** (1993).
- [29] T. Brabec, and F. Krausz, *Rev. Mod. Phys.* **72** (2000).
- [30] K. J. Schafer *et al.*, *Phys. Rev. Lett.* **70** (1993).
- [31] T. N. Rescigno, *Modern Electronic Structure Theory* (World Scientific, Singapore, 1995), Vol. 1.
- [32] B. I. Schneider, and T. N. Rescigno, *Physical Review A* **37** (1988).
- [33] T. N. Rescigno, B. H. Lengsfeld, and A. E. Orel, *Journal of Chemical Physics* **99** (1993).